OROGRAPHICALLY INDUCED CYCLOGENESIS: ANALYSIS OF NUMERICAL EXPERIMENTS*

A. Buzzi**, P. Malguzzi, S. Tibaldi***

Istituto di Fisica "A. Righi" dell'Università di Bologna, Italy

* This paper has been submitted for publication elsewhere and has been reproduced here because it was presented by one of the authors (S. Tibaldi) at the Mountain Workshop.

** Laboratorio per lo Studio dei Fenomeni Fisici e Chimici della Bassa e Alta Atmosfera - C.N.R. Bologna, Italy.

*** European Centre for Medium Range Weather Forecasts, Shinfield Park, Reading, U.K.

ABSTRACT:

Cyclogenesis induced by an isolated mountain chain in a baroclinic flow is simulated in a channel version of the HIBU (Mesinger-Janjić) primitive equation model. The main features characteristic of cyclogenesis in the lee of the Alps are reproduced when the mountain interacts with a finite amplitude baroclinic wave. The distribution of derived quantities like vertical velocity and potential vorticity compare well with those analyzed in case studies.

The intercomparison of the evolution of the various fields and the analysis of energetics in experiments with and without mountains highlights the nature of the physical processes involved.

A small scale baroclinic process is responsible for an amplification of the initial disturbance produced by the mountain when the cold front, associated with the large scale wave, moves over it. This process, though enhancing the local energy conversion, reduces the efficiency of the baroclinic conversion over the whole domain.

1. Introduction

The dynamical influence of orography on atmospheric flows has been the subject of many investigations in recent years. It involves important phenomena ranging from forcing of planetary scale waves to local effects like short lee waves, foëhn, etc. A major effect of large mountain complexes on the synoptic scale, intermediate to those mentioned, is the formation of lee cyclones that strongly affect the weather and climate of particular geographical sectors (Petterssen, 1956). The Western Mediterranean, situated in the lee of mountain chains in the case of northerly or north-westerly winds, is a striking example of such a cyclogenetic region.

It is well known that the Alps in particular play a primary role in the generation of these cyclones. They can either remain in the formation area or drift away. Cyclogenesis in the lee of the Alps (CLA, also known as Genoa cyclogenesis), which shows features different from cyclogenesis in the lee of long ridges like the Rockies or the Andes, is characterized by an essentially three-dimensional deformation of the thermal and wind fields due to the limited horizontal extension of the Alpine chain (CENFAM, 1961-65, Radinović, 1965, Buzzi and Tibaldi, 1978, hereafter mentioned as BT).

In this paper we describe numerical experiments devised with the aim of simulating this particular kind of cyclogenesis. Because of the complexity of the phenomenon, only tentative explanations based on the analysis of phenomenology have been so far proposed (see, for a discussion, Speranza, 1975, and Tibaldi, 1979).

The BT case study indicates that cyclogenesis in the lee of the Alps is the result of a baroclinic instability process triggered by the deformation of the thermal fields in the low troposphere produced by the Alps when a cold front impinges on them coming from the north-west. This cold front is usually associated with a "primary" cyclone moving eastwards over

Central Europe. The initial deepening of a trough aloft seems more a condition for the further development of the initially shallow disturbance than a consequence of it. However lee cyclogenesis eventually results in a localization and reinforcing of the trough in the middle and upper troposphere, possibly leading to the formation of a cut-off low.

Much effort has been devoted to the numerical simulation of CLA, with various degrees of success. Either real data or idealized conditions have been used to initialize the experiments. The first noteworthy, and remarkably successful, attempt to model CLA is due to Egger (1972).

He uses a six level primitive equation sigma model, in a channel domain. The initial condition simulates a cyclonic vortex over North-western Europe, embedded in a baroclinic westerly current. The difficulty of incorporating a steep mountain in a rather coarse mesh width (350 km) has been overcome by Egger by representing the Alps with a vertical barrier 3000 km high. Along this "wall" the normal velocity component vanishes, so that the barrier exerts a blocking effect on the low-level flow. Although this method of treating orography could appear rather crude since slope effects are not represented, it seems to work much better than the other one commonly used, which consists in the smoothing of the real topography over the grid size. This indicates that the horizontal deformation of the flow and the differential advection in the vertical produced by the barrier are fundamental mechanisms of CLA.

The role of the low level deformation of the wind and thermal fields has been subsequently confirmed in a numerical experiment produced by Trevisan (1976), relevant to the problem of CLA. Trevisan's model is a channel version of a six level primitive equation model in isentropic coordinates. A ridge extending in the west-east direction, with a gap in it, is introduced as an idealization of the Alps-Pyrenees system. A baroclinic wave is allowed to develop from an initial disturbance superimposed to an atmosphere containing a westerly jet structure.

When the resulting cyclone moves north of the model Alps, the cold outbreak associated with it can penetrate through the gap simulating the region of the Rhone valley, while cold advection is retarded, more to the east, by the barrier. A new cyclone hence forms south of the "Alps", associated with this distortion of the cold front. The cyclone is confined to the lowest layers, but there is evidence of a southward deviation of the upper jet consistent, as pointed out by the author, with the enhanced cold advection through the gap, via the thermal wind relationship.

Numerous forecasts of CLA have been produced starting from initial conditions based on real data. We will mention, among others, those presented by Bleck (1977), Mesinger and Janjić (1977), Capaldo and Finizio (1977), Tibaldi and Janjić (1977), Mesinger et al. (1979). The general impressio drawn from these experiments is that the forecasting skill of the models increases together with their ability in represent the real features of topography (steepness in primis) and in limiting spurious response to steep orography, which acts as a typical generator of computational noise. However the main failure that these model exhibit (with the exception of Mesing et al., 1979) is a poor forecast of the mid and upper tropospheric developments. As a consequence shallower and shorter-lived cyclones than in reality are produced. An inadequate representation of the topography is not the only cause of thi problems arise also from things like the use of artificial boundary conditions (limited area models) and the lack of parameterization of condensation effects and of subgrid scale processes. An attempt to overcome some of these limitations discussed in Mesinger et al. (1979).

The experiments we present here are idealized simulations. T have been performed with the aim of isolating simple mechanism and extending the clarifying conclusions drawn from previous experiments and analyses of real data. Some difficulties usually encountered in real case studies (diagnosis of derive

fields like vertical velocity, energy conversion, etc.) can be at least partially overcome by a diagnosis of the numerical experiments, provided that the essential features of the phenomenon that we want to study are captured.

We have tried to keep the initial and boundary conditions as simple as possible having in mind the interaction of a large scale baroclinic wave, containing a well developed frontal system, with a mountain resembling the Alps in shape, height, orientation and latitudinal location.

2. The model

The model is a channel version of the HIBU model, which has been developed as a joint effort of the Federal Hydrometeorological Institute of Yugoslavia and of the University of Belgrade (Mesinger, 1973; Mesinger and Janjić, 1974; Mesinger, 1977; Mesinger and Janjić, 1977).

It is a 5-layer primitive-equation model in sigma coordinates, which has been designed for the specific purpose of limited area, short range forecasts in regions of steep topography. Here we simply list the main characteristics of the model; for more details the reader is referred to the literature mentioned above.

The horizontal grid is semi-staggered with geographic coordinates; the domain used here ranges from 30 to 66° N, with a longitudinal extension of 60°. The mesh widths are 1.5x1° longitude-latitude (grid distance of about 160 km in middle latitudes).

In the vertical σ is defined equal to zero at 200 mb, with the three uppermost layers spaced of $\Delta\sigma = 0.25$ and the two lower layers of $\Delta\sigma = 0.125$.

Forward-backward time integration is used (Mesinger, 1977), together with a method (Mesinger, 1973) that avoids the formation of false two-grid-interval waves; forward integration is applied to the advection terms, which conserves vorticity, kinetic energy and enstrophy within the non-divergent part of horizontal motion. The time step used in the experiments shown here is 360 s. The hydrostatic error in the pressure-gradient force in the presence of steep σ-surfaces is minimized with a method devised by Janjić (1977). Vertical transport of momentum, surface friction and dry convective adjustment are included while neither radiative nor moist processes are treated. The surface drag coefficient (as in Bleck, 1977) and the eddy exchange coefficient increase with the surface elevation in order to simulate the enhanced drag expected over rough mountainous terrain. The coefficient

simply vary linearly with height:

$$K = K_o(1+h)$$

where h is the tropographic height in km.

3. The experiments

In order to simulate the interaction of the Alps with a cold front associated with a mature baroclinic wave, a wave is allowed to develop for 96 hours in the channel with a flat lower boundary, and then the mountain is introduced, which grows to its full amplitude in 8 hours. This procedure, although rather artificial, has the advantage of allowing a realistic flow pattern to interact with the mountain. If the mountain is introduced from the beginning (this procedure was adopted by Egger, 1972), one needs to specify an initial condition for lee cyclogenesis that cannot represent all the features of a mature baroclinic wave, including frontal structures. On the other hand, if a baroclinic wave grows from a small disturbance in the presence of a mountain, its development is severely distorted from the beginning (Trevisan, 1976) and one cannot obtain in this way a clean "pre-cyclogenetic" situation like that simulated in our experiments.

The initial state has been defined by imposing a meridional temperature gradient varying as a hyperbolic tangent of latitude ($\Delta T = 35.6^{o}K$ between the northern and southern boundaries at the surface).

Static stability increases with height above 300mb and more to the north, in order to simulate a smooth transition betwee tropospheric and stratospheric air; in this way the meridiona temperature gradient decreases with height and at 200mb is reduced to about one fourth of its value at the ground, but no reverse of its sign occurs.

The velocity is set to zero at the surface and obtained elsewhere through the thermal wind equation. In this way a westerly jet-like structure is initially produced, with maximum wind at 200mb. Pressure is prescribed by superimposing a barotropic sinusoidal perturbation over the basic baroclinic pressure field ($\bar{p}$ = 1000mb at the ground). The

zonal and meridional wavelengths of the perturbation are set equal to the zonal and twice the meridional lengths of the channel respectively, so that the perturbation vanishes at the northern and southern boundaries. Along the northern and southern boundaries all the variables are kept constant and equal to their initial values during the subsequent integration. Variables at points on the lines immediately adjacent to these boundaries are calculated by averaging between the inner points, where integration is performed, and the boundary points. Cyclic conditions are imposed at the lateral boundaries, involving five meridional lines. Fig. 1 shows the situation after 96 hours of integration; all quantities have been interpolated from σ-surfaces to isobaric surfaces. A wave of quite large amplitude has developed and is still growing (note the westward tilting with height). A pronounced frontal structure can be observed in the temperature field at 850 mb. The entire picture seems realistic enough to represent the situation favourable for initiation of CLA, if the Alps are thought to be located ahead of the cold front, south of the cyclone centre at the surface. In fact at this instant the mountain shown in Fig. 2 starts growing. Its shape and height resemble those of the Alps, but with a slight exaggeration in the horizontal extent. The orientation is also slightly different from that of the Alps, and has been chosen in order to have the larger cross-section with respect to the advancing cold front. Actually CLA is most likely to occur when a cold front advances almost perpendicularly to the longitudinal direction of the Alpine chain.

A control experiment has been run with flat ground, for comparison. The mountain and control experiments will be indicated hereafter by C and M respectively.

The growth of the mountain in our simulation does not produce dramatic effects between 96 and 120 hours. After 120 hours a pressure perturbation appears at the surface in exp. M confined to the mountain region and consisting of an upwind

high-lee low system superimposed on the large scale pressure field. This pressure perturbation is a characteristic of flow across the Alps and always appears in the early stages of CLA, but should not be confused with it (Egger, 1972; Speranza, 1975; BT).

Approximately at 120 hours the low level cold front reaches the top of the mountain, as appears in the temperature field at 850 mb in Fig. 3. It is from this instant that the cyclogenetic process starts. After 132 hours (Fig. 4) the lee cyclone firstly appears with closed circulation both at the surface and at 850 mb. The ridge of high pressure upwind of the mountain has developed further, and the isobars are crowded together along the relief. The cold front has intensified and slowed down in the mountain region; cold advection is confined only to the regions south-west and north-east of the mountain (Fig. 4b). In exp. C at the same instant (Fig. 5) only the primary cyclone is present at the surface, and it is about 10 mb deeper than in exp. M. The trough south of it coincides with the position of the cold front, which has moved eastwards without any hindrance. Similar features can be seen in the two maps at 850mb. At this level in exp. M the air is cooler upstream and warmer downstream of the mountain than in exp. C. Upstream the temperature is even lower than along the northern boundary, implying adiabatic cooling due to rising motion. More to the north-east the front is weaker in M than it is in C.

At 500mb the differences between the two experiments are less pronounced. In exp. M a weaker development of the trough in the north and a westward shift can be observed with respect to exp. C. In correspondence to the low level lee cyclone no significant deepening is yet observed. However, over the mountain region an important difference can be noticed in the advection field. In fact, while in exp. C cold advection prevails also east of the trough in the geopotential field,

in exp. M cold advection is confined to the west and the south of the mountain, while warm advection is present above the lee side (it has been verified that this conclusion is valid not only for geostrophic advection, evident in Fig. 4c, but also for real wind advection).

We expect therefore mass divergence aloft over the lee region, consistently with the pressure fall at the ground. Upper divergence in CLA has been observed (Dinies, 1938) and held responsible, together with the retardation of cold advection in the lower layers, for the formation of the depression at the surface (Ficker, 1920; Scherhag, 1965; Radinović, 1965). Egger (1972) found strong divergence aloft in the lee of his model Alps, accompanied by convergence at low levels, during most of the cyclogenetic period.

After 144 hours the lee cyclone reaches its maximum intensity near the surface (Fig. 6). At the ground the shape and position of the cyclone are roughly the same as in Fig. 4a, but the pressure minimum has dropped to 978mb, 16mb lower than in exp. C at the same position and instant.

To the north-west of the mountain pressure has increased further. The primary cyclone has moved slightly north-eastwards, maintaining the same intensity, in contrast with exp. C, where this cyclone continues its deepening. Also at 850mb the lee cyclone is well pronounced. It has developed its own thermal wave, with a cold front in the south, produced by the advance of cold air that has been deviated around the southern edge of the mountain. This is the model equivalent of the cold outbreaks in the Rhone Valley associated with real CLA, but is not as strong as those, perhaps because of the lack of the Pyrenees and the action of the southern boundary. Near the north-eastern edge of the mountain a very strong temperature gradient has formed, as a result of the confluence between cold air moving eastwards around the mountain and warm air advected from the south by the cyclonic circulation. This frontogenetic effect has been observed also

in real case studies (BT). The situation after 156 hours of integration is shown in Fig. 7 for exp. M and in Fig. 8 for exp. C. In Fig. 7a it can be seen that the lee cyclone at the surface has now started to drift away from the region of formation, while filling up (pressure in the minimum has risen 8mb in 12 hours). At the same time cold air is breaking into the depression moving around the north-eastern edge of the mountain, as seen at 850mb. Adiabatic cooling has continued along the northern side, perhaps to such an extent to become rather unrealistic. This suggests that in the model the flow over the mountain is overestimated, that is the model Alps are not high or steep enough to force the air to flow around rather than over them.

While at the ground and, to a lesser extent, at 850mb the cyclone intensity has decreased, at 500mb it has continued to increase, resulting, at this instant, in the appearance of a closed geopotential minimum. This is a noteworthy result, having in mind the general difficulty of numerical models to predict the development aloft. It should be noted, however, that the closed minimum at 500mb appears only 24 hours after the cyclone has formed at the ground, while in cases of intense CLA this time lag is generally shorter (6-12 hours). At 500mb cold advection now also affects the southern part of the lee region; warm advection is still present more to the north. This pattern is consistent with that of a baroclinic wave in the mature stage.

Let us now examine more closely the overall effects of the mountain 60 hours after its appearance, by comparing the two experiments at 156 hours. The general impression is that the baroclinic development has been split by the mountain into two parts, distinct in position and scale, the lee cyclone having both horizontal and vertical scales smaller than those of the primary cyclone. Furthermore, it is evident at all levels that the development of the primary cyclone, i.e. o the wave already present at 96 hours, is substantially reduced by this splitting. A redistribution of the energy conversion processes is therefore implied, as it will be confirmed by

the analysis of the energetics presented in section 5. The temperature distribution at low levels is also very different in the two experiments. It can be seen in Fig. 7 and 8 that at 850mb the air in the large region south-east of the mountain, is generally warmer in exp. M than in exp.C and that the opposite is true in the region north-west of the mountain. These differences are due not only to warming and cooling in the vicinity of the mountain and related to the forced vertical motion, but also to the retardation of the cold advection in the large scale flow. There is, therefore, evidence that the mountain has an influence on scales much larger than its horizontal extent. In view of the striking similarity between the lee cyclogenesis simulated in exp. M and real CLA, we have drawn the conclusion that the basic mechanisms acting in reality are included in the model development, and therefore we have proceeded to a parallel diagnosis of exp. M and C in order to shed some light on these mechanisms.

A third experiment can be mentioned here, which was done identically to exp. M, but with a straight mountain instead of an arc shaped one, oriented parallel to the oncoming cold front. Lee cyclogenesis did occur also in this case, though slightly weaker than in exp. M. This result does not contradict that of Egger (1972), who did not produce cyclogenesis when substituting his arc-shaped Alps with a straight barrier. In fact this barrier in his experiments was oriented in the east-west direction, having therefore little blocking effect on the cold outbreak.

We can conclude that the arc shape of the Alps is favourable for cyclogenesis, but is not strictly necessary.

4. Vertical velocity, vorticity and potential vorticity

Fields of $\omega \equiv \frac{Dp}{Dt}$ have been plotted every 12 hours at 850 and 500mb, interpolating from σ-surfaces. After 120 hours the vertical velocity at 500mb does not show substantial differences between the two experiments. Rising motion prevails east and sinking motion west of the trough. On the contrary at 850mb, as expected, the influence of the mountain is evident (Fig. 9). The forcing effect of sloping terrain on the horizontal wind can account for most of the differences in the ω-fields between exp. M and C. General rising motion is observed on the north-west slope, where cold air impinges upon the mountain. Another region of ascent is present south of the eastern edge, where pre-frontal south-westerly flow is forced to rise. Similarly, descending motion is present east of the southern edge and north-east of the other. Vertical motion is determined elsewhere by the large scale dynamics, with maximum ascent in advance of the northern portion of the cold front and maximum descent in the rear of the southern part of it. Small scale waves appear in the field; they seem not to be produced by the mountain since they are also present in exp. C.

Twelve hours later the vertical motion in the vicinity of the mountain presents a more organized structure. Direct forcing by the sloping terrain is now weaker, because the flow has readjusted so as to become almost parallel to the contour lines of the ground. The structure of vertical motion now seems to be more consistent with baroclinic development which begins at about 132 hours. In fact, at 850mb the strongest descent is now observed south of the mountain, where cold advection is present; correspondingly, the maximum ascent is located near the north-eastern edge, where warm advection is produced by the circulation of the incipient cyclone. At 500mb the vertical motion confirms the hypothesis of divergent motion at upper levels above the lee region, since strong ascending motion is observed there.

Fig. 10 shows the ω-fields after 144 hours. The patterns are very similar to those at 132 hours, but slightly shifted to the east, and with stronger values at the maxima.

At 850mb sinking motion now covers all the near lee region, while at 500mb upward motion still prevails in the vicinity of the north-eastern edge of the mountain. The "dipoles" of vertical velocity in Fig. 10 visualize very clearly the scale of the lee development, which is about one half of that of the primary wave. If we compare the vertical velocity structure with the temperature and advection fields (Fig. 6), we can notice again, qualitatively, the correlation indicating a process of slantwise convection (a quantitative evaluation will be presented in the next section). At this stage the development appears self-sustained and quite independent of the presence of the mountain. In exp. C at the same instant the ω-field shows only upward motion in advance of the cold front and of the occlusion in the north, and descending motion (weaker than in exp. M) above the eastern part of the low level anticyclone.

After 156 hours in exp. M (maps not shown) the vertical motion pattern is still similar to that after 144 hours, but has drifted to the east and vertical velocities, particularly in the region of ascent, are weaker, indicating that the baroclinic conversion process has decreased.

One could now wonder how the patterns of vertical velocity exhibited by the model compare with those deduced from observations. A maximum of ascending motion above the region south-east of the Alps, which has correspondence in Fig. 10, seems statistically confirmed by the high precipitation index in that region during cases of CLA. More precise evidence can be found in the analysis of vertical motion reported in BT. Moreover, in Fig. 11 analyses of vertical velocity in the Alpine region during the case of CLA of 25-26 Nov. 1977 are shown (Buzzi and Pümpel, work in progress). These vertical velocities have been computed on the θ-surface 292°K with

the isentropic trajectory method, based on radiosonde data. They are therefore not completely reliable because of the insufficient resolution provided by these data in comparison with the time-space scales of the phenomenon and because of the adiabatic assumption. However, if we compare Fig. 11a with Fig. 9 and Fig. 11b with Fig. 10 (the height of the isentropic surface 292^{o}K ranges from 4500 to 2000m in the region), we can observe quite a good similarity. In particula the structure of forced vertical motion near the Alps, mentioned for Fig. 9 can be seen also in Fig. 11a, which corresponds to the incipient stage of cyclogenesis. Twelve hours later (Fig. 11b) the vertical velocity is more organized on the scale of the developed lee cyclone, as in Fig. 10.

In conclusion, the existence of two stages of evolution emerge from the analysis of the vertical motion. In the first stage, when the cold front is impinging the model Alps on the north-western side, the pre-frontal flow (sketched in Fig. 2) is forced by the sloping terrain to sink in the region denoted by A in the figure, and to rise in the region denoted by B. Therefore a "dipole" of vertical motion form in the region south-east of the mountain, because of the particular correlation between the horizontal velocity and the orography, which have opposite curvature. In the second stage the front moves over the mountain, but slower than in the surrounding region. The temperature and advection fields become correlated, in this process, with the pre-existent field of vertical velocity so as to release available potential energy. A positive feedback process in response to the initial orographic disturbance is suggested by the fact that the pattern of vertical motion in the lee region organizes and reinforces without any essential change of the position of positive and negative centres while the front advances and the cyclone grows.

We will only mention briefly the diagnoses of other fields, such as wind, vorticity and potential vorticity. The wind field shows clearly at low levels the deviating effect of the mountain. As expected, the strongest departures from quasi-geostrophy are observed near the mountain. At higher levels

the jet tends to split into two branches, one passing south and the other north of the mountain, in agreement with observations (Danielsen, 1973; BT).

The evolution of the vorticity fields reflects clearly the formation of the lee cyclone. At 850mb after 144 hours in the lee region positive values up to $1.7 \times 10^{-4} S^{-1}$ are observed. Also at 500mb at 144 and 156 and, to a lesser extent, even at 132 hours the cyclonic vorticity maximum is concentrated over the region, unlike exp. C, where the cyclonic vorticity is weaker and more distributed along the cyclonic side of the north-westerly and south-westerly jets. Of particular interest is the distribution of potential vorticity at 500mb. In case studies of intense CLA (Danielsen, 1973) evidence was produced of tropopause folding over the western Mediterranean, with associated downward transport of high values of potential vorticity from the stratosphere. Tibaldi and Trevisan (1973) found the presence of isolated maxima of potential vorticity in the mid troposphere in the region south of the Alps after cyclone formation. This behaviour is confirmed in our experiments: in Fig. 12 the distributions of potential vorticity at 500mb after 156 hours in exp. M and C are shown. Large values in exp. M over the mountain region must have been advected from higher levels, where static stability was higher in the initial state. This agrees with the stronger downward motion seen at 500mb in exp. M along the south-west part of the trough. It should be noticed that potential vorticity is not strictly conserved by the numerical schemes of this model, and therefore that it cannot be used as a reliable tracer; nevertheless, the differences between exp. M and C are significant enough to diagnose a mountain influence also at high levels.

5. Energetics

In order to gain a more quantitative understanding of the processes that intervene in the formation of the lee cyclone, we have computed the kinetic energy budgets. Consider the equation expressing the total change of specific kinetic energy for a single pressure level:

$$\frac{DK}{Dt} = -\underset{\sim}{V}_R \cdot \nabla\phi - \underset{\sim}{V}_D \cdot \nabla\phi + D \qquad (1)$$

Where $\frac{D}{Dt} = \underset{\sim}{V}\cdot\nabla + \omega\frac{\partial}{\partial p}$, ϕ is the geopotential, D is a dissipation term and $\underset{\sim}{V}$, the horizontal wind vector, has been split into the rotational (V_R) and divergent (V_D) parts.

This splitting enables us to look separately at the barotropic and baroclinic conversion processes, respectively (Pearce, 1974; Chen and Wiin-Nielsen, 1976; Chen, Alpert and Schlatter, 1978). Eq. (1) can be integrated over a horizontal area A. In an open domain, after application of the continuity equation, we get:

$$\frac{\partial}{\partial t}\int_A K\ ds + \int_A \nabla(K\underset{\sim}{V})ds + \int_A \frac{\partial}{\partial p}(\omega K)\ ds = \qquad (2)$$

$$= -\int_A \underset{\sim}{V}_R.\nabla\phi ds - \int_A \underset{\sim}{V}_D.\nabla\phi ds + \int_A D\ ds$$

We have computed the various terms of eq. (2) (except the dissipation term) in exp. M and C for different pressure levels every 12 hours from 96 to 156 in the area shown in Fig. 2, which embraces the lee cyclone. The separation between divergent and non-divergent wind has been obtained by means of an iterative method devised by Endlich (1967) and used also in the analysis by Chen, Alpert and Schlatter (1978).

In Fig. 13a and 13b the evolution in time of the first two

terms of the RHS of eq(2) are shown at 850 and 500mb respectively. These two levels are chosen as representative of the lower troposphere, where the influence of the mountain is direct, and of the mid and upper troposphere respectively. In fact, at any level below approximately 650mb, the behaviour is similar to that of Fig. 13a, while above this level it is similar to that of Fig. 13b. We notice in Fig. 13a that the barotropic contribution at 850mb is slightly reduced by the presence of the mountain in the area considered. On the contrary the baroclinic conversion, which in exp. C remains small in that area, in exp. M becomes dominant after about 132 hours, with a considerable peak at 144 hours.

What has been previously deduced by observation of the temperature and ω-fields is now quantitatively confirmed. At 500mb the picture is different. Both the barotropic (which is the most important at this level) and the baroclinic contributions are substantially reduced by the presence of the mountain. This is not in contrast with the higher values of vorticity in M than in C at 500mb; the presence of a closed minimum of geopotential in exp. M also means a local minimum of kinetic energy (in fact, mean kinetic energy in M is lower than in C in the area considered) at 500mb, and this can be consistent with a lower energy production. However, this implies that the mechanisms that are responsible for the kinetic energy production in the lower layers between 132 and 156 hours (exp. M) remain confined at low levels. In this respect, the baroclinic development appears to be rather shallow, in agreement with its small horizontal scale (shallow and small relatively to the scales of the primary wave). In Table 1 the kinetic energy budget for exp. M is shown, averaged in the layer between 925 and 675mb and integrated over the limited area shown in Fig. 2. The local change of specific kinetic energy has been computed using centered differences in 24 hour intervals. Dissipation is deduced as a residual. Analogous computations have been made for the upper layers and for exp. C. Table 1 shows that kinetic energy almost doubles between 108 and 144 hours with maximum

growth between 120 and 144 hours. At 108 and 120 hours energy production is essentially due to the barotropic term, while, afterwards, the baroclinic term prevails, as already seen for the 850mg level. Kinetic energy is exported at all times both horizontally and vertically. Horizontal outflow decreases in time, while the vertical one increases, with a maximum at 144 hours which reflects the prevailing of upward motion in the area.

It is interesting, at this point, to see what the effect of the mountain is on the energy conversion over the whole domain.

If integration of eq.(2) is performed over the entire area of the domain, the 2nd LHS and 1st RHS terms vanish so that only the baroclinic term is responsible for the global energy conversion. The evolution in time of this term is plotted in Fig. 13c. At 500mb the global baroclinic conversion is reduced to about one half by the presence of the mountain for the entire period considered, though the relief occupies a relatively small area of the domain. At 850mb (exp. M) the conversion is initially reduced; it is higher than that in exp. C only at 144 and 156 hours, when the contribution of the lee development becomes dominant in the overall budget, over-compensating for the weaker development of the primary wave.

These results provide more evidence that the influence of the mountain is important also on the large scale.

6. Conclusions

The lee cyclogenesis induced in our numerical experiment by the perturbing effect of a steep obstacle of horizontal scale of the order of 1000 km reproduces quite realistically the phenomenon known as cyclogenesis in the lee of the Alps. Analysis of the various fields and of the energy budget confirms previous ideas based on case studies and numerical experimentation. In particular, the conclusion advanced in BT, that we are in the presence of a baroclinic development triggered by the perturbing action of the orography, seems to be proved by our experiments. It is shown, in fact, that a substantial conversion of available potential into kinetic energy takes place in the lower half of the lee troposphere during the growth phase of the cyclone. This process occurs at the expense of baroclinic conversion on larger vertical and horizontal scales.

An inspection of the vertical velocity field shows that on the side of the mountain where the cyclone forms a dipole of vertical motion is induced in the first stages by direct orographic forcing on the cyclonically curved flow. At the same time, the temperature field is deformed by the obstacle, in such a way that vertical velocity and temperature gradually become positively correlated for baroclinic development.

In this process a positive feedback mechanism can be recognized, which leads to the release of instability. This instability seems to be of the conditional type, since a finite amplitude disturbance is required to trigger it.

It will be the aim of future work to investigate the dependence of the orographic disturbance upon the geometry of the obstacle and the atmospheric parameters, and to determine under which conditions its amplitude is sufficient to trigger the cyclogenetic process.

Acknowledgements

We are indebted to Prof. F. Mesinger and Dr. Z. Janjić for placing the HIBU model at the authors' disposal and for helpful suggestions.

We are grateful also to Dr. H. Pümpel, Dr. A. Speranza and Dr. A. Trevisan for valuable comments and to Dr. A. Simmons for reading the manuscript.

This work was supported by C.N.R. in the frame of "Progetto Finalizzato Promozione Qualità dell'Ambiente".

References

Bleck, R. 1977 "Numerical simulation of lee cyclogenesis in the Gulf of Genoa", Mon. Wea. Rev., 105, 428-445.

Buzzi, A. and Tibaldi, S. 1978 "Cyclogenesis in the lee of the Alps: A case study", Quart.J.R.Met.Soc., 104, 271-287.

Capaldo, M. and Finizio, S. 1977 "Fine-mesh model experiments in the Mediterranean area", Paper presented at first Planning Meeting, GARP, Mountain Sub-Progr., Venice.

CENFAM 1961-1965 "Research work on the project 'Cyclone development in the lee of the Alps', STR 1,2,3,4,5,6,8. Istituto di Fisica dell'Atmosfera, Roma.

Chen, T.C., Alpert, J.C. and Schlatter, T.W. 1978 "The effects of divergent and non-divergent winds on the kinetic energy budget of a mid-latitude cyclone: a case study", Mon.Wea.Rev., 106, 458-468.

Chen, T.C. and Wiin-Nielsen, A. 1976 "On the kinetic energy of the divergent and nondivergent flow in the atmosphere", Tellus, 28, 486-498.

Danielsen, E. 1973 "Cyclogenesis in the Gulf of Genoa". In "Mesoscale Meteorological Phenomena", Proc. of the Summer School CNR, Laboratorio per lo Studio della Dinamica delle Grandi Masse, Venice, 189-192.

Dinies, E. 1938 "Die Entstchung der Genua zyklone am 11.2.1938. Ann.Hydro.Mar. Met., 466-569.

References (contd.)

Egger, J.	1972	"Numerical experiments on the cyclogenesis in the Gulf of Genoa", Beitr. Phys. Atmos., 45, 320-346.
Endlich, R.M.	1967	"An iterative method for alterir the kinetic properties of wind fields", J. Appl. Meteor., 6, 837-844.
Ficker, H.V.	1920	"Der Einfluss der Alpen auf die Fallgebiete des Luftdrucks und die Entschung der Mittel-meerdepressionen", Met. Z., 37 360-373.
Janjić, Z.I.	1977	"Pressure gradient force and advection scheme used for fore-casting with steep and small scale topography", Beitr. Phys Atmos., 50, 186-199.
Mesinger, F.	1973	"A method for construction of second-order accuracy differen schemes permitting no false tw grid-interval wave in the heig field", Tellus, 25, 444-457.
Mesinger, F.	1977	"Forward-beckward scheme, and i use in a limited area model", Beitr. Phys. Atmos., 50,200-21
Mesinger, F. Strickler, R., Sirutis, J. and Chludzinski, J.	1979	"Numerical simulation of Genoa cyclogenesis, including cut-of in the upper troposphere", Euromech colloquium: "Airflow over hills and mountains", München, 2-5 April 1979.
Mesinger, F. and Janjić, Z.I.	1974	"Noise due to time-dependent boundary conditions in limited area models". The GARP Progr. on Numer. Experiment,4, 31-32.
Mesinger, F. and Janjić, Z.I.	1977	"Numerical problems related to effect of mountain and forecas of Genoa cyclogenesis". Paper presented at the First Plannin Meeting - GARP Mountain Sub-pr Venice.

References (contd.)

Pearce, R.P. 1974 "The design and interpretation of diagnostic studies on synoptic-scale atmospheric systems". Quart.J.R. Met. Soc., 100, 265-285.

Petterssen, S. 1956 "Weather analysis and forecasting" McGraw-Hill Book Co., Vol.1, 266-272.

Radinović, D. 1965 "On forecasting of cyclogenesis in the West Mediterranean and other areas bounded by mountain ranges by baroclinic model". Arch.Meteor.Bioklimatol. A 14, 279-299.

Scherhag, R. 1965 "On the reciprocal influences between oceans, continents and the atmosphere and their effect on the general circulation". Proc. Int.Symp.Syn.Large-scale Proc. in the Atmos., Moscow, 233-255.

Speranza, A. 1975 "The formation of baric depressions near the Alps". Ann. Geofis., 28, 177-217.

Tibaldi, S. 1979 "Cyclogenesis in the lee of orography and its numerical modelling, with special reference to the Alps". Submitted for publication in the GARP Report "Orographic effects in planetary flows".

Tibaldi, S. and Janjić, Z.I. 1977 "Cyclogenesis in the lee of the Alps: some numerical experiments". Paper presented at first Planning Meeting GARP Mountain Sub-Progr., Venice.

Tibaldi, S. and Trevisan, A. 1973 "Application of a geostrophic NWP model in isentropic coordinates to the study of cyclogenesis in the Ligurian Sea". In "Mesoscale Meteorological

References (contd.)

Phenomena". Proc. of the Summer School, CNR, Laboratori per lo Studio della Dinamica delle Grandi Masse, Venice, 274-278.

Trevisan, A. 1976 "Numerical experiments on the influence of orography on cyclone formation with an isen tropic primitive equation mode J.Atmos.Sci.,33, 768-780.

Figure Captions

Fig. 1 : situation after 96 hours of integration, when the mountain is inserted.

a) Surface pressure (last two digits of the value in mb);

b) Geopotential (dm) and temperature (^{o}C) at 850mb;

c) Geopotential and temperature at 500mb.

Fig. 2 : Bottom topography for exp. M. Dashed: area in which the kinetic energy budget is calculated. For other symbols see sect. 4.

Fig. 3 : exp. M, 120 hours, 850mb.

Fig. 4 : exp. M, 132 hours, a) surface; b) 850mb; c) 500mb.

Fig. 5 : as in Fig. 4, but for exp. C.

Fig. 6 : exp. M, 144 hours. a) surface; b) 850mb.

Fig. 7 : exp. M, 156 hours. a) surface; b) 850mb; c) 500mb.

Fig. 8 : as in Fig. 7, but for exp. C.

Fig. 9 : exp. M, ω at 850mb, 120 hours (MKS units; positive values: descending motion).

Fig.10 : exp. M, 144 hours. a) ω at 850mb; b) ω at 500mb.

Fig.11 : vertical velocity (cm/s; positive: ascending motion) computed at θ = 292^{o}K.

a) 25 Nov. 1977, 15 GMT; b) 26 Nov. 1977, 03 GMT.

Fig.12 : potential vorticity ($x10^{-8}$MKS units), 156 hours, 500mb. a) exp. M; b) exp. C.

Fig.13 : energy conversion terms integrated over the limited area of Fig. 2 (a : 850mb and b : 500mb) and on the whole domain (c).

Table 1: kinetic energy budget integrated over the limited area of Fig. 2 and averaged in the layer between 925 and 675mb.

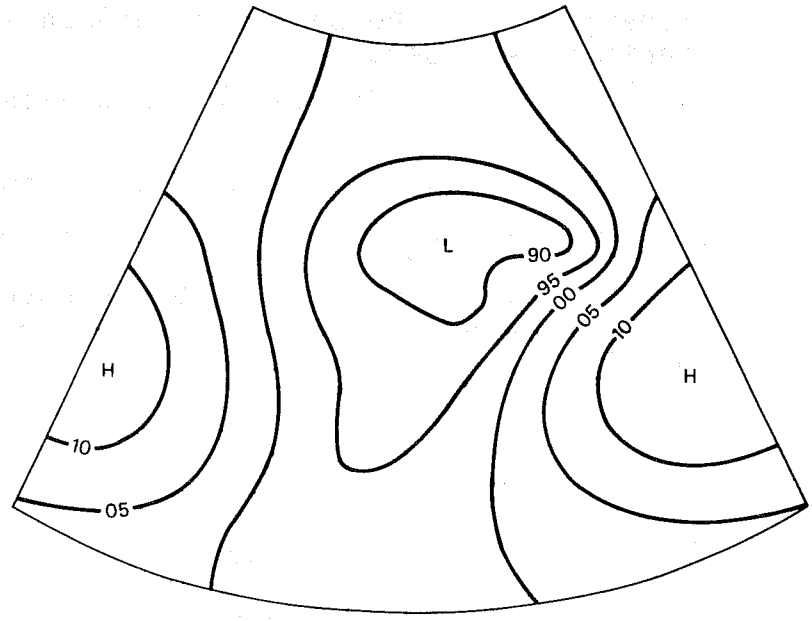

Fig. 1a Situation after 96 hours of integration, when the mountain is inserted. Surface pressure (last two digits of the value in mb).

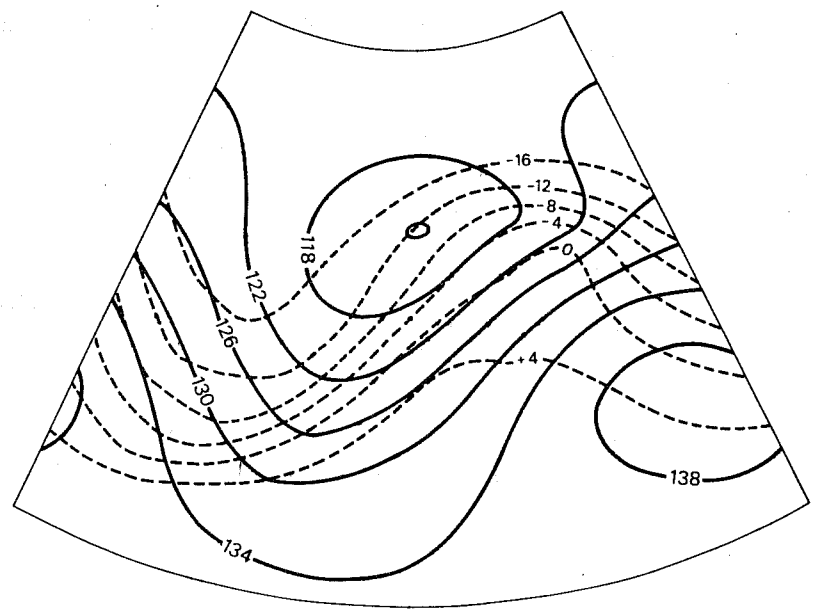

Fig. 1b Situation after 96 hours of integration, when the mountain is inserted. Geopotential (dm) and temperature (^{o}C) at 850 mb.

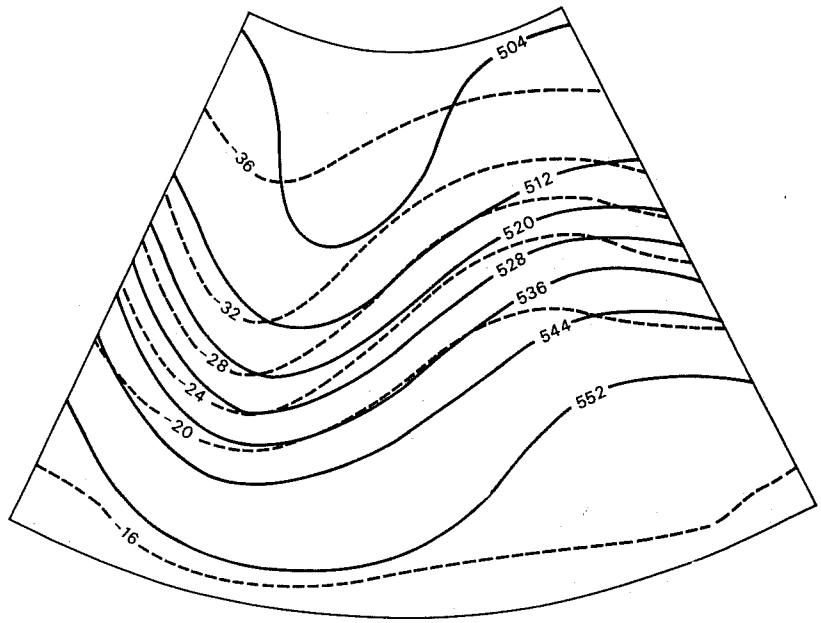

Fig. 1c Situation after 96 hours of integration, when the mountain is inserted. Geopotential and temperature at 500 mb.

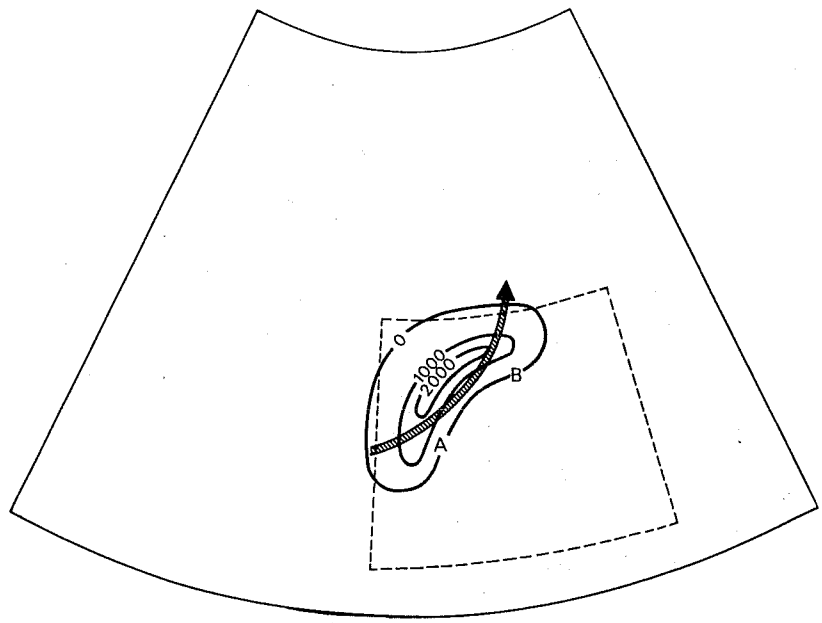

Fig. 2 Bottom topography for exp. M. Dashed: area in which the kinetic energy budget is calculated. For other symbols see Sect. 4.

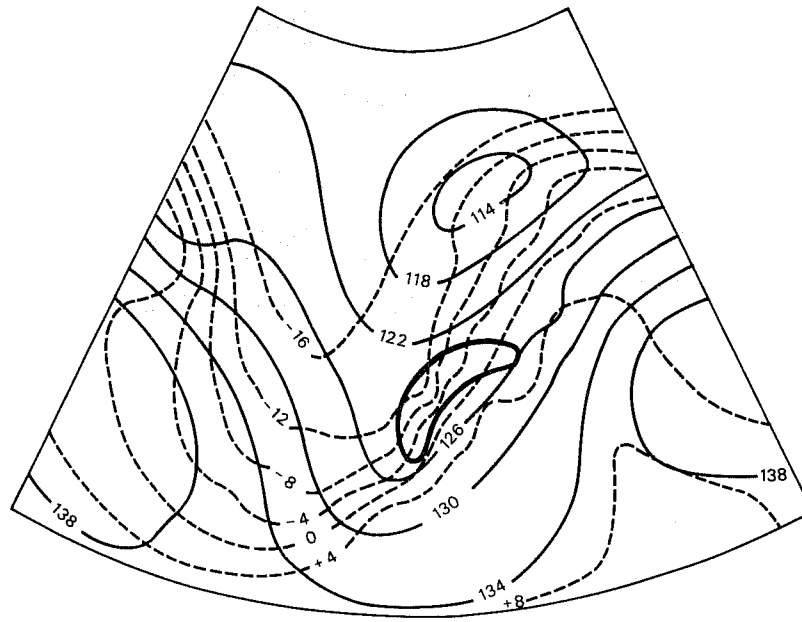

Fig. 3 Exp. M, 120 hours, 850 mb.

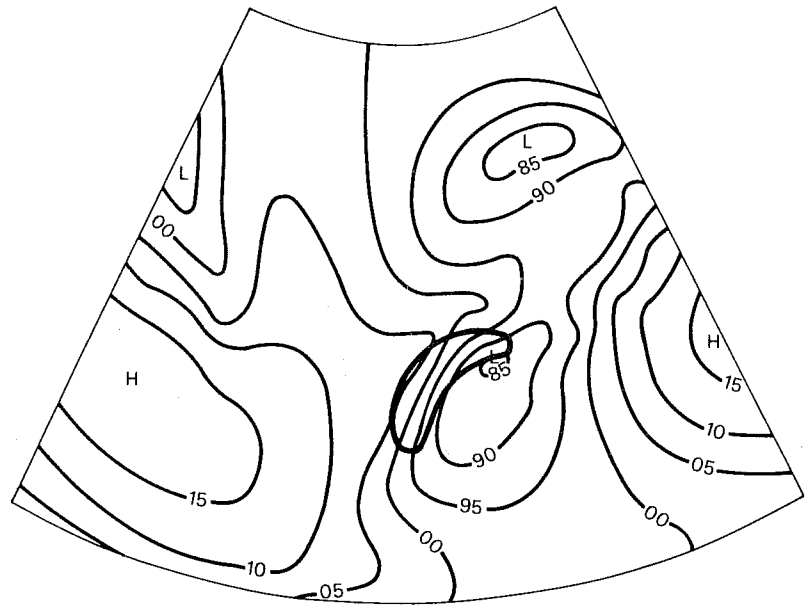

Fig. 4a Exp. M, 132 hours, surface.

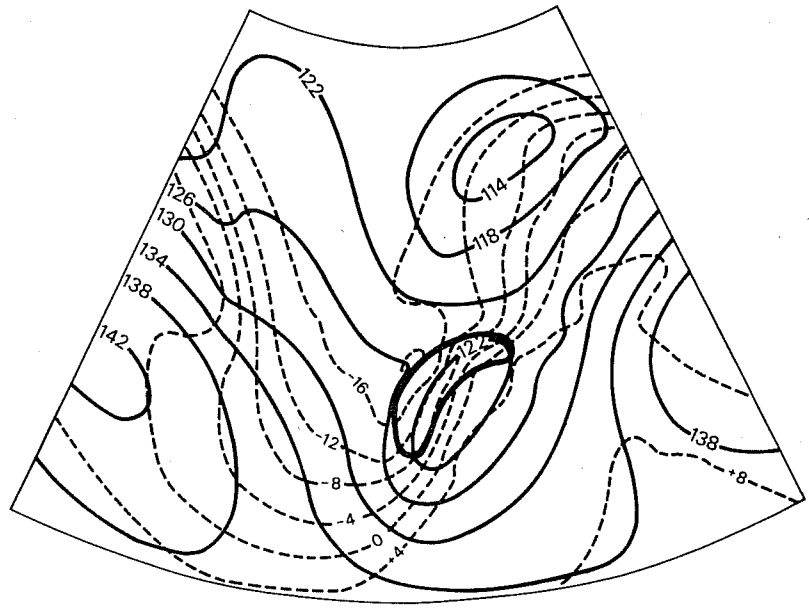

Fig. 4b Exp. M, 132 hours, 850 mb.

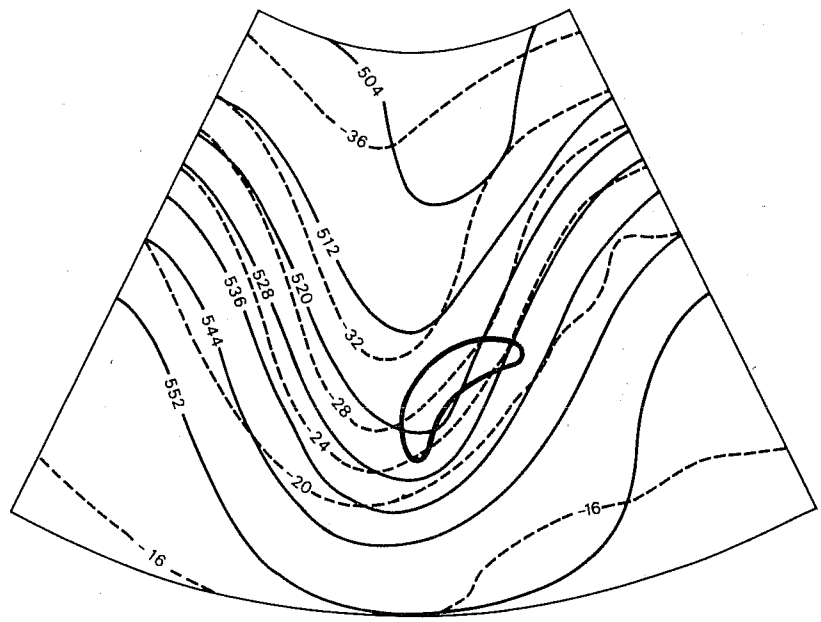

Fig. 4c Exp. M, 132 hours, 500 mb.

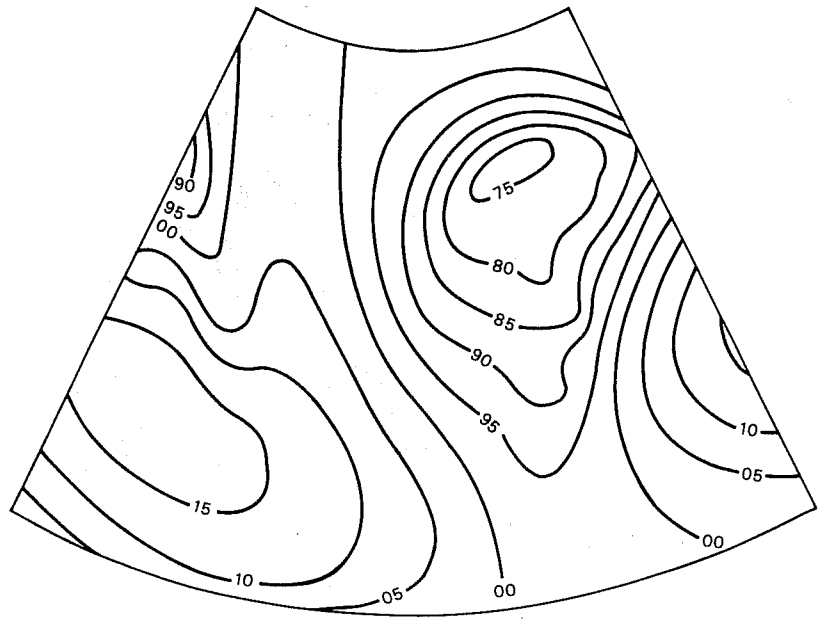

Fig. 5a As in Fig. 4a, but for exp. C.

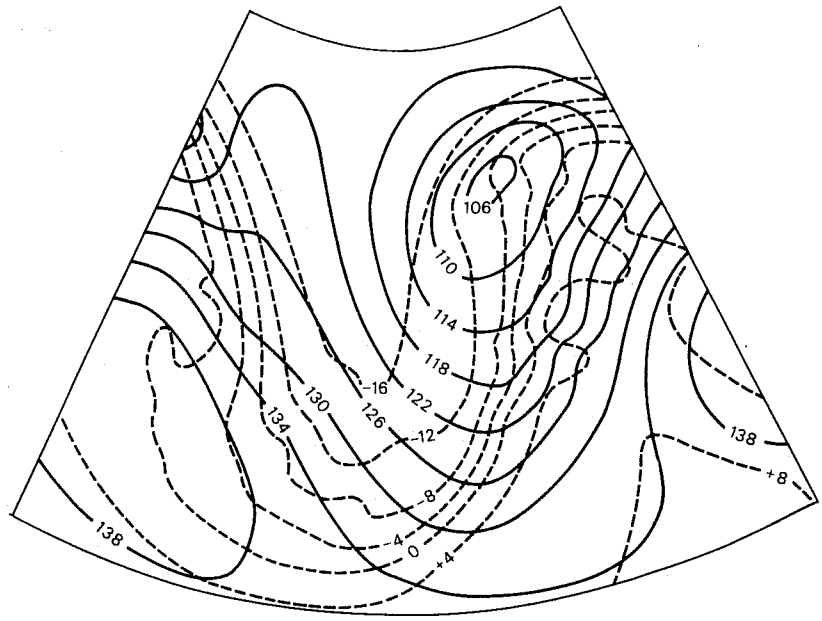

Fig. 5b As in Fig. 4b, but for exp. C.

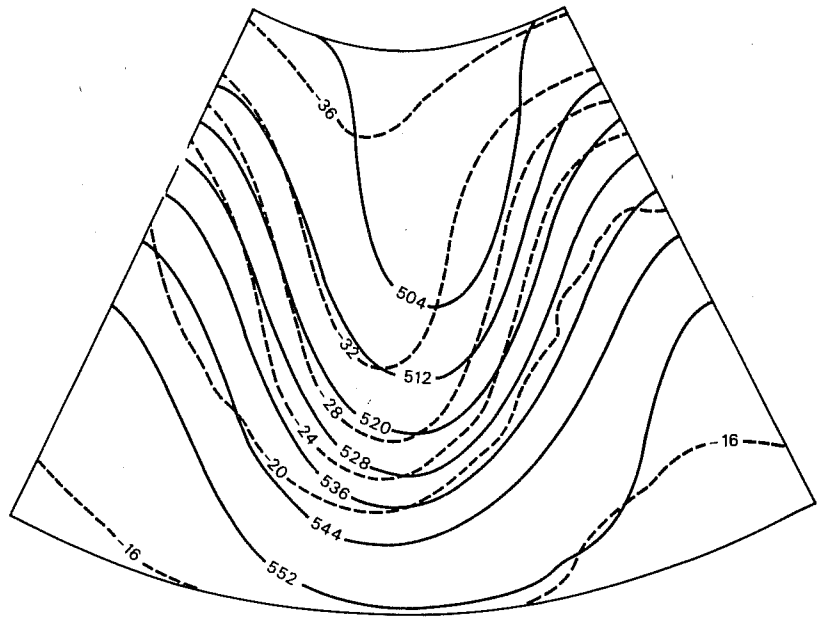

Fig. 5c As in Fig. 4c, but for exp. C.

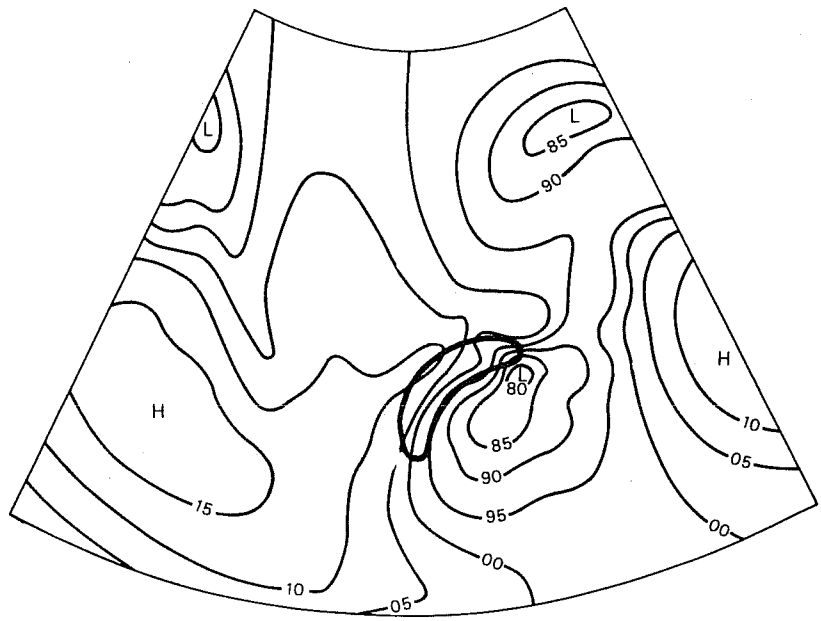

Fig. 6a Exp. M, 144 hours, surface.

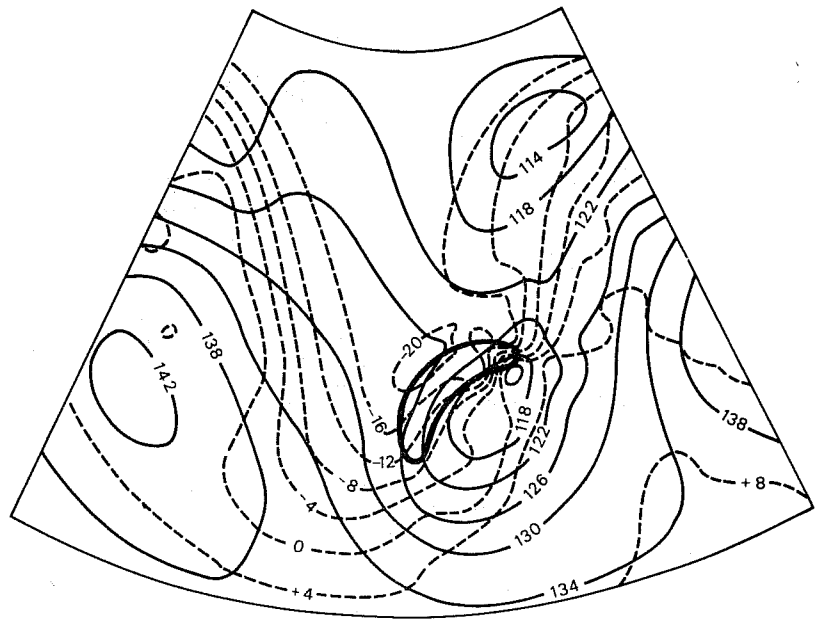

Fig. 6b Exp. M, 144 hours, 850 mb.

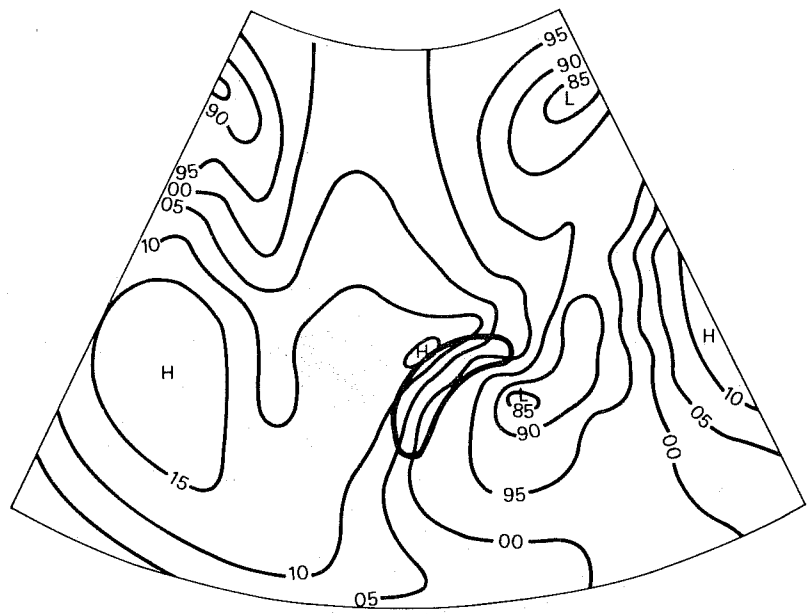

Fig. 7a Exp. M, 156 hours, surface.

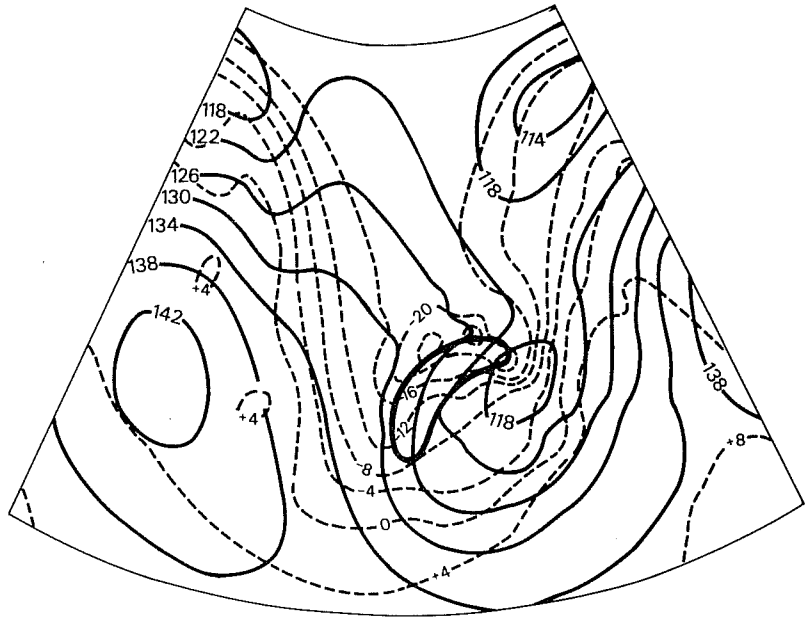

Fig. 7b Exp. M, 156 hours, 850 mb.

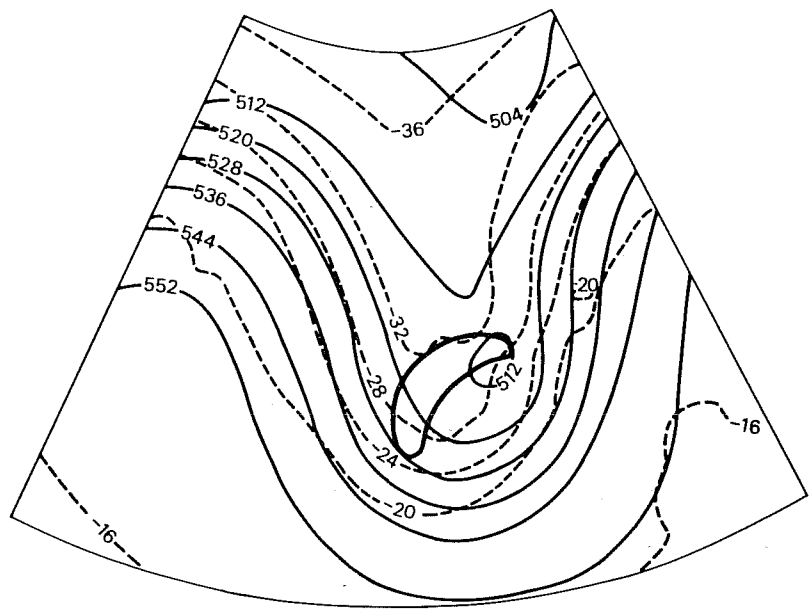

Fig. 7c Exp. M, 156 hours, 500 mb.

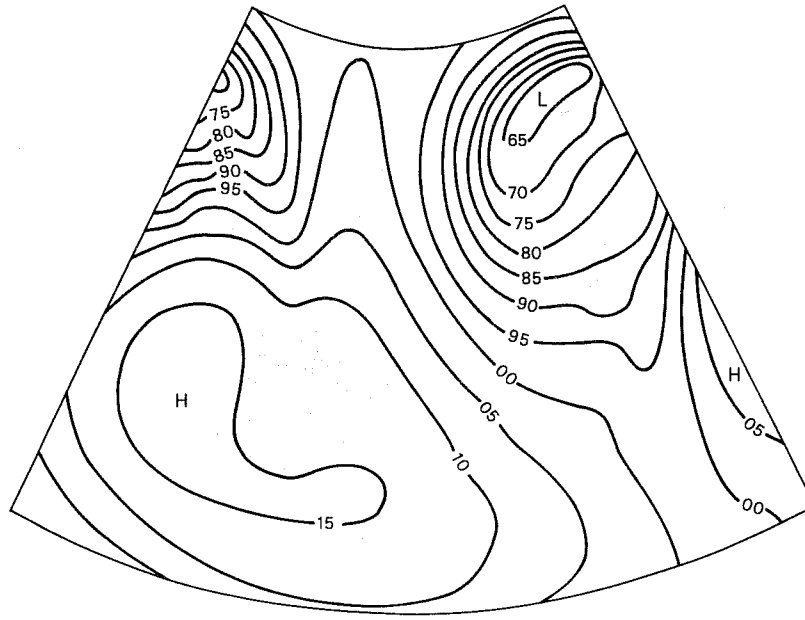

Fig. 8a As in Fig. 7a, but for exp. C.

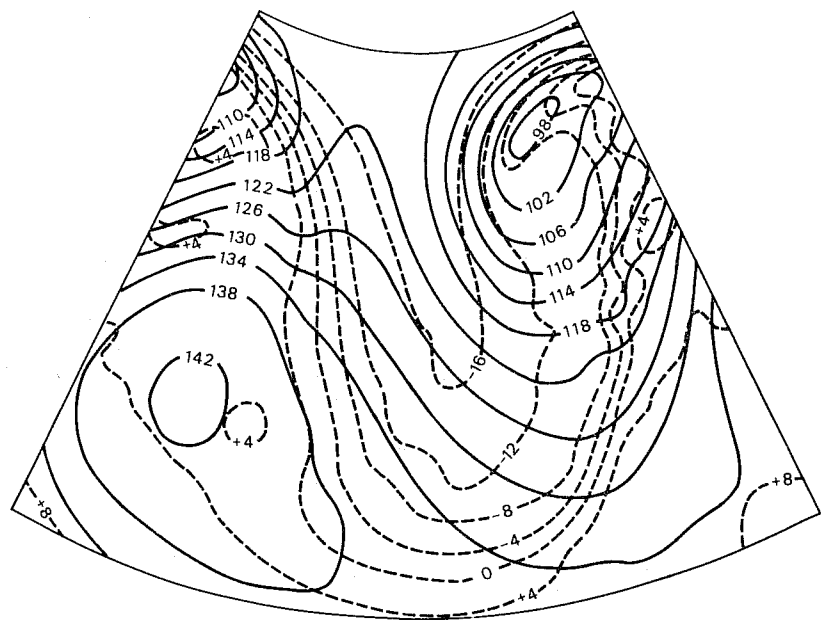

Fig. 8b As in Fig. 7b, but for exp. C.

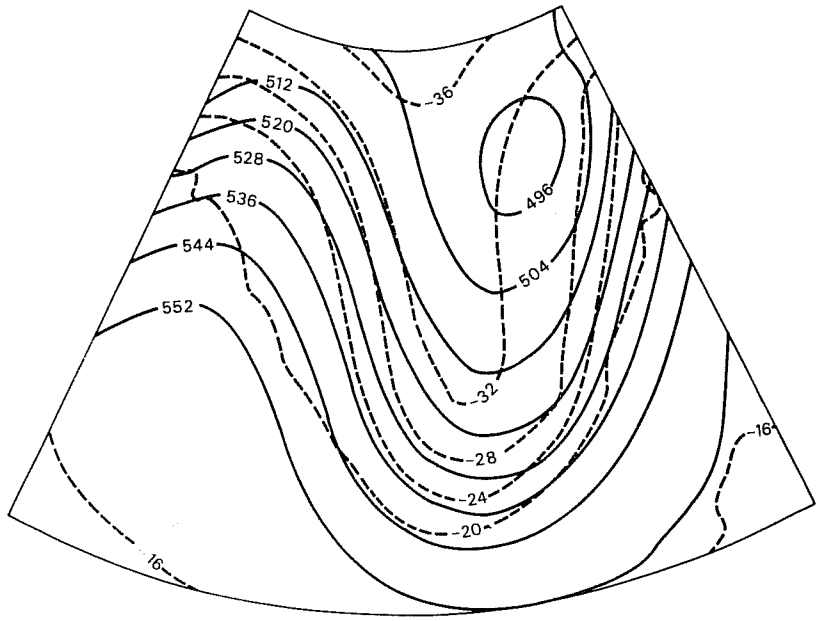

Fig. 8c As in Fig. 7c, but for exp. C.

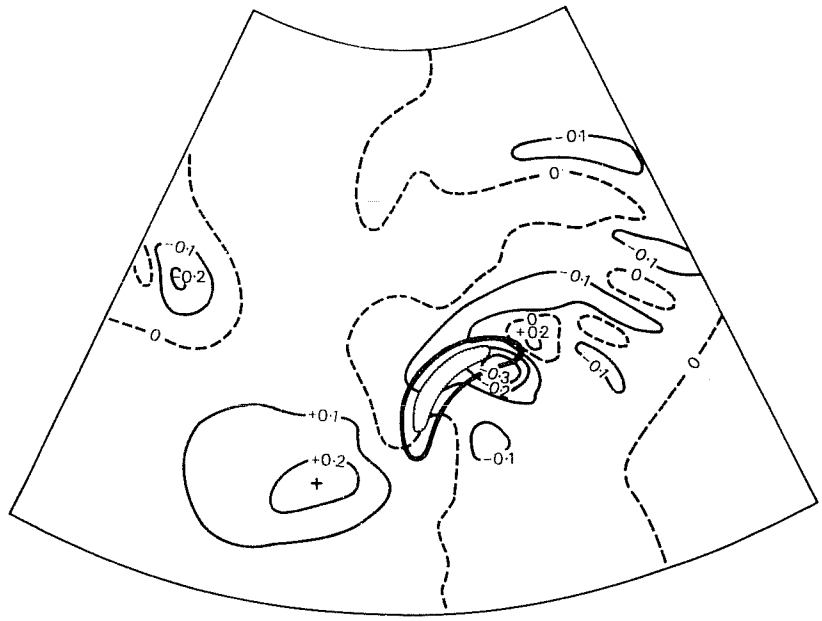

Fig. 9 Exp. M, ω at 850 mb, 120 hours (MKS units; positive values: descending motion).

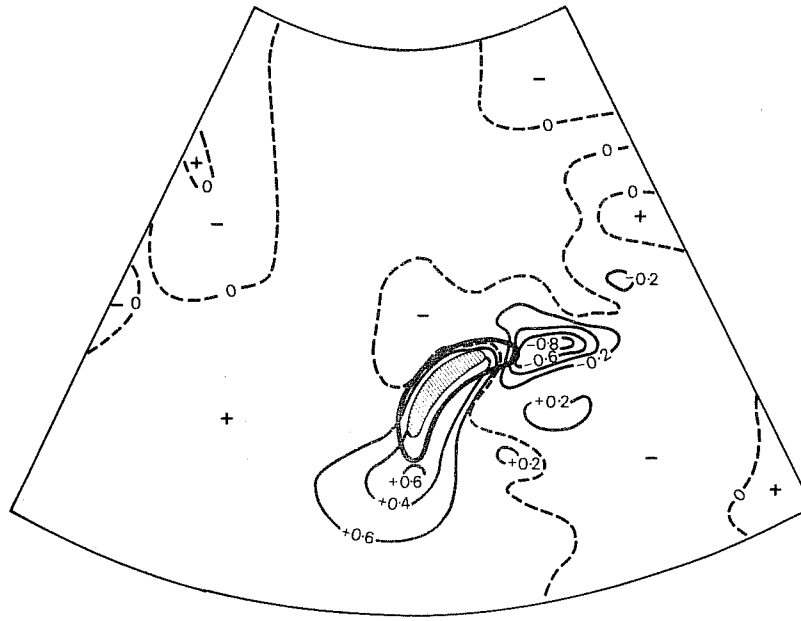

Fig. 10a Exp. M, 144 hours, ω at 850 mb.

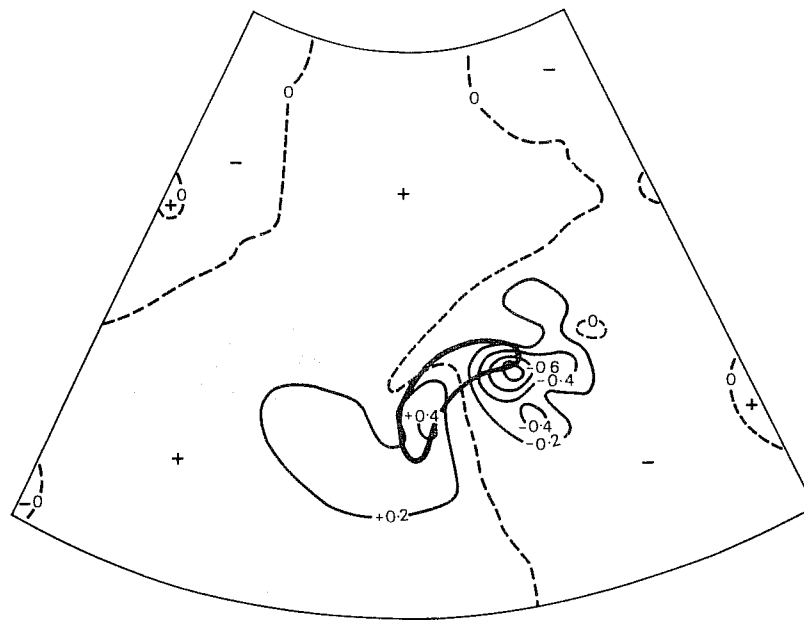

Fig. 10b Exp. M, 144 hours, ω at 500 mb.

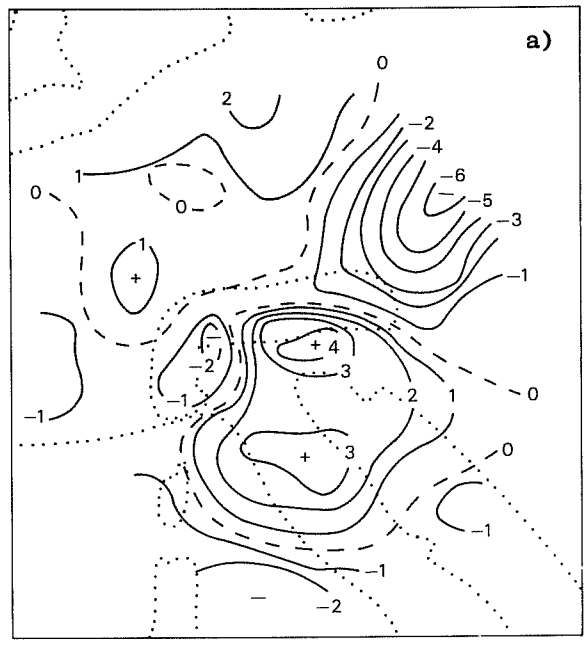

Fig. 11 Vertical velocity (cm/s; positive: ascending motion) computed at θ = 292 °K.

a) 25 Nov. 1977, 15 GMT
b) 26 Nov. 1977, 03 GMT

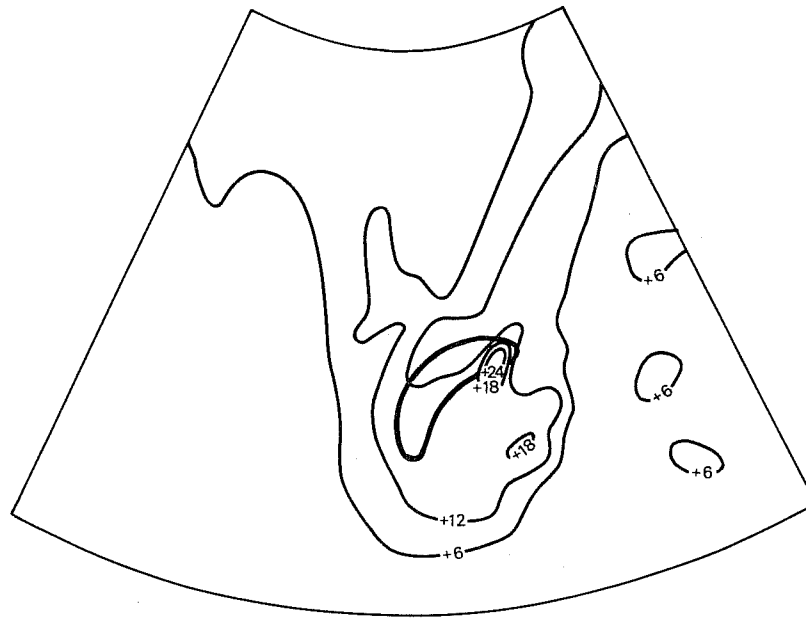

Fig. 12a Potential vorticity ($x10^{-8}$ MKS units), 156 hours, 500 mb, exp. M.

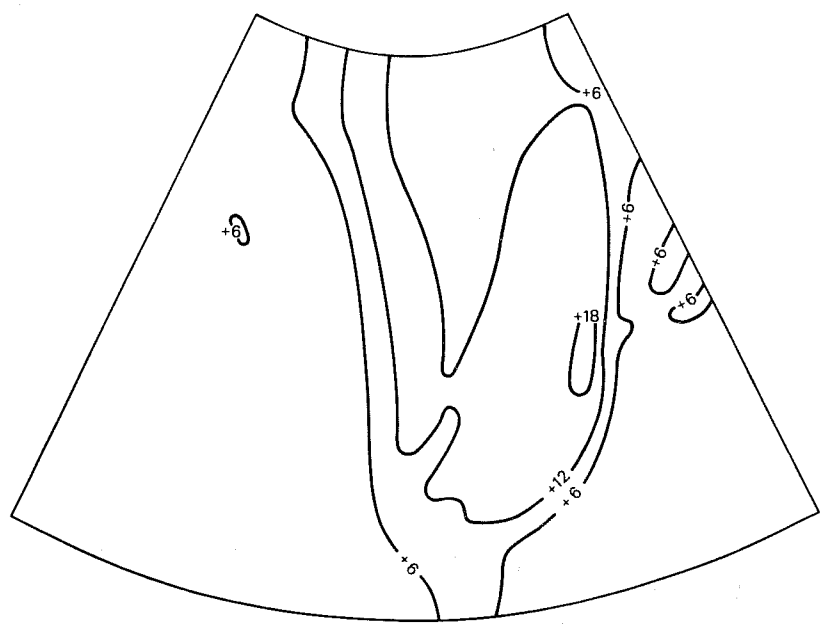

Fig. 12b Potential vorticity ($x10^{-8}$ MKS units), 156 hours, 500 mb, exp. C.

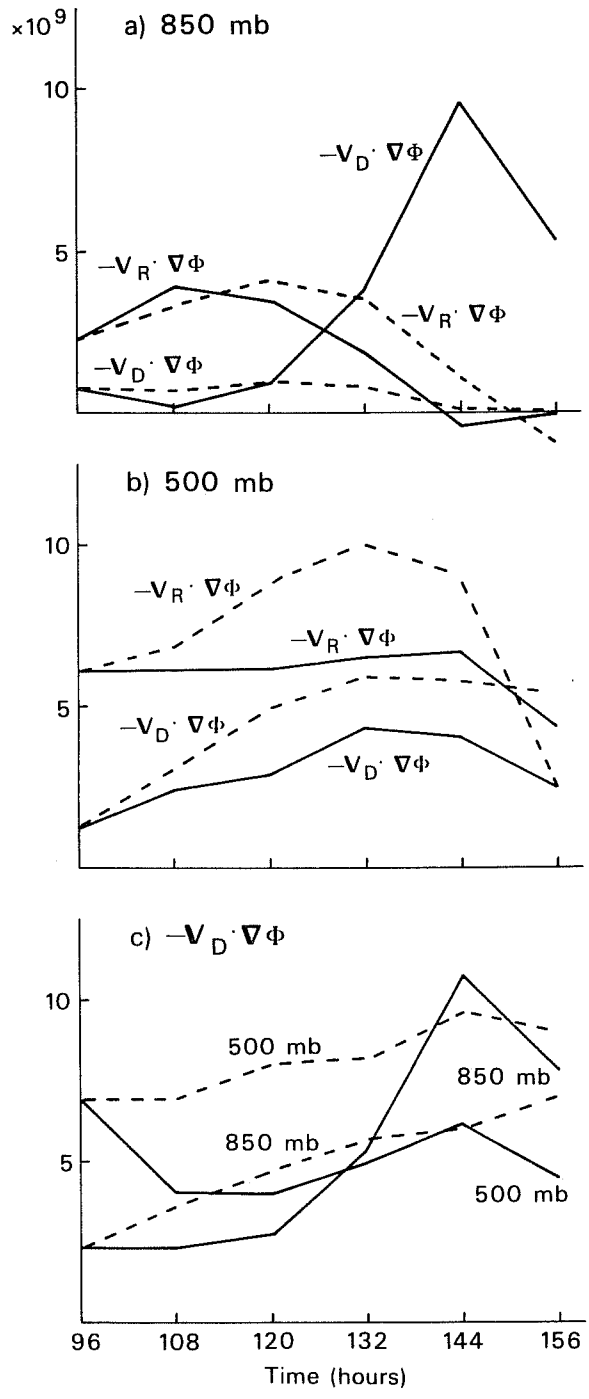

Fig. 13 Energy conversion terms integrated over the limited area of Fig. 2 (a): 850 mb and b): 500 mb) and on the whole domain(c).

TIME h	K $\times 10^{-14}$	$\partial K/\partial t$ $\times 10^{-9}$	$\nabla(KV)$ $\times 10^{-9}$	$\frac{\partial}{\partial p}(\omega K)$ $\times 10^{-9}$	$-V_R \cdot \nabla\phi$ $\times 10^{-9}$	$-V_D \cdot \nabla\phi$ $\times 10^{-9}$	Res.
96	2.2	-	1.4	0.6	2.8	1.0	-
108	2.2	0.5	1.7	1.3	4.4	0.9	-1.8
120	2.6	1.4	1.5	0.9	3.6	0.9	-0.7
132	3.4	1.7	1.4	1.3	2.5	3.6	-1.7
144	4.1	0.7	0.4	2.0	0.9	7.9	-5.7
156	4.0	-	0.8	1.7	0.3	5.7	-

Table 1. Kinetic energy budget integrated over the limited area of Fig. 2 and averaged in the layer between 925 and 675 mb.